



THE UNIVERSITY *of* EDINBURGH

Edinburgh Research Explorer

3D interpolation in wave-based acoustic simulation

Citation for published version:

Bilbao, S 2021, '3D interpolation in wave-based acoustic simulation', *IEEE Signal Processing Letters*, vol. 29, pp. 384-388. <https://doi.org/10.1109/LSP.2021.3137750>

Digital Object Identifier (DOI):

[10.1109/LSP.2021.3137750](https://doi.org/10.1109/LSP.2021.3137750)

Link:

[Link to publication record in Edinburgh Research Explorer](#)

Document Version:

Peer reviewed version

Published In:

IEEE Signal Processing Letters

Publisher Rights Statement:

© 2021 IEEE. Personal use of this material is permitted. Permission from IEEE must be obtained for all other uses, in any current or future media, including reprinting/republishing this material for advertising or promotional purposes, creating new collective works, for resale or redistribution to servers or lists, or reuse of any copyrighted component of this work in other works.

General rights

Copyright for the publications made accessible via the Edinburgh Research Explorer is retained by the author(s) and / or other copyright owners and it is a condition of accessing these publications that users recognise and abide by the legal requirements associated with these rights.

Take down policy

The University of Edinburgh has made every reasonable effort to ensure that Edinburgh Research Explorer content complies with UK legislation. If you believe that the public display of this file breaches copyright please contact openaccess@ed.ac.uk providing details, and we will remove access to the work immediately and investigate your claim.



3D Interpolation in Wave-based Acoustic Simulation

Stefan Bilbao, *Senior Member, IEEE*

Abstract—In any acoustics simulation setting relying on computation over a spatial grid, interpolation of the acoustic field is essential in order to accurately model source and receiver positions. Most available approaches to 3D interpolation, such as those used in computer graphics or medical imaging, are based on polynomial or windowed-sinc designs. In this short contribution, it is shown that highly accurate optimised designs are available if particular features of acoustic wave propagation and numerical scheme design are incorporated: performance can be tuned to an acoustic wavenumber range of interest, taking into account numerical dispersion artefacts, and the interdependence of the solution to the acoustic wave equation at neighbouring time steps can be further exploited, leading to extremely compact locally-defined interpolation designs. Numerical results are presented.

Index Terms—FDTD, finite difference time domain method, 3D interpolation, room acoustics, wave-based simulation

I. INTRODUCTION

Wave-based acoustic simulation refers to the numerical solution of the acoustic wave equation over an enclosure. For volumetric time-domain methods, the acoustic field is represented over a grid in three dimensions. The finite difference time domain method (FDTD) is the most well-known method [1], [2], [3], [4], but there are many other varieties [5], [6] [7], [8]. Such methods are heavily used in virtual room and architectural acoustics [9], [10], [11], [5], [7], [8], environmental acoustics [12], and in ultrasound applications [13], [14], [15]. In most practical settings, the grid is chosen to be regular (often Cartesian), allowing for simplified algorithm design and opportunities for massive parallelisation.

In virtually all practical applications, interpolation over the 3D grid is necessary. This includes the readout from the acoustic field at arbitrary locations and the dual problem of point source modeling. Interpolation plays a key role in scattering problems using techniques such as the immersed boundary method that rely on point-like forcing terms at non-grid locations [16], including in acoustics [17]. The majority of 3D interpolation techniques are used in computer graphics [18], medical imaging applications [19] and ocean dynamics [20], and are not adapted particularly to problems in acoustics.

Relative to applications involving the interpolation of measured datasets, in acoustic simulation, there is not normally a full resampling of a 3D field—rather, interpolation is performed at a limited number of locations (typically for input and output, but also for modeling scattering surfaces). Furthermore, interpolants are ideally spatially compact, so as to avoid interference with boundary conditions. A special concern in virtual acoustics is the possibility of dynamic (moving) source/receiver modeling for walkthroughs. In simulation, new

concerns about numerical error emerge, that can be used to inform optimization criteria, and new possibilities for improved performance are available due to the interdependence of the solution to the wave equation at neighbouring time steps.

In this article, 3D interpolation is framed in terms of an optimization in the Fourier domain, tunable against the useful wavenumber range of the particular numerical method employed, leading to compact interpolation designs with low error over a specified range, following preliminary results presented earlier in [21] in the context of source modeling. Error can be reduced further by employing values computed at neighbouring time steps. Comparisons against standard interpolation methods are presented.

II. VOLUMETRIC WAVE-BASED SIMULATION

As a simple but representative scenario, consider the following wave-based acoustics problem including input and output:

$$\frac{1}{c^2} \partial_t^2 p - \Delta p = \delta^{(3)}(\mathbf{x} - \mathbf{x}_{\text{in}}) f(t) \quad (1a)$$

$$p_{\text{out}}(t) = p(\mathbf{x}_{\text{out}}, t) = \iiint_{\mathcal{D}} \delta^{(3)}(\mathbf{x} - \mathbf{x}_{\text{out}}) p dV \quad (1b)$$

Here $p(\mathbf{x}, t)$ is the acoustic pressure in Pa, as a function of time $t \in \mathbb{R}$, and for $\mathbf{x} \in \mathcal{D} \subset \mathbb{R}^3$. c is the wave speed in $\text{m} \cdot \text{s}^{-1}$. ∂_t represents partial differentiation with respect to time t , and Δ is the 3D Laplacian operator. $f(t)$ is an input waveform driving the system at location $\mathbf{x} = \mathbf{x}_i$, activated through a three-dimensional Dirac delta function $\delta^{(3)}$. An output waveform $p_{\text{out}}(t)$ is drawn from the acoustic field at $\mathbf{x} = \mathbf{x}_{\text{out}}$, an operation which can similarly be expressed in terms of a Dirac delta function selecting the output location. Given the duality of input and output as shown above, only output will be considered in the remainder of this paper.

In a numerical setting, consider a discrete time volumetric method defined over a regular Cartesian grid, of spacing X m and with time step T s. The grid function p_1^n represents an approximation to $p(\mathbf{x}, t)$ at $\mathbf{x} = \mathbf{l}X$ and $t = nT$, where integer $n \geq 0$ is the time index, and $\mathbf{l} \in \mathcal{D}_d \subset \mathbb{Z}^3$ is the spatial grid index. A large family of two-step schemes may be written as:

$$p_1^{n+1} = 2p_1^n - p_1^{n-1} + \lambda^2 L p_1^n \quad p_{\text{out}}^n = \mathcal{I}(\mathbf{x}_{\text{out}}) p_1^n \quad (2)$$

Here, $\lambda = cX/T$ is the Courant number and L approximates the Laplacian (scaled by X^2) and has the general form:

$$L p_1^n = \sum_{\nu=1}^V \sum_{\mathbf{e} \in \mathbb{P}(\mathbf{v}_\nu)} b_\nu (p_{1+\mathbf{e}}^n - p_1^n) \quad (3)$$

Such a Laplacian approximation includes, in its stencil, V separate shells of adjacent grid points, defined over signed permutations \mathbb{P} of non-negative integer-valued 3-vectors \mathbf{v}_ν , $\nu = 1, \dots, V$, with weighting coefficients b_ν , $\nu = 1, \dots, V$.

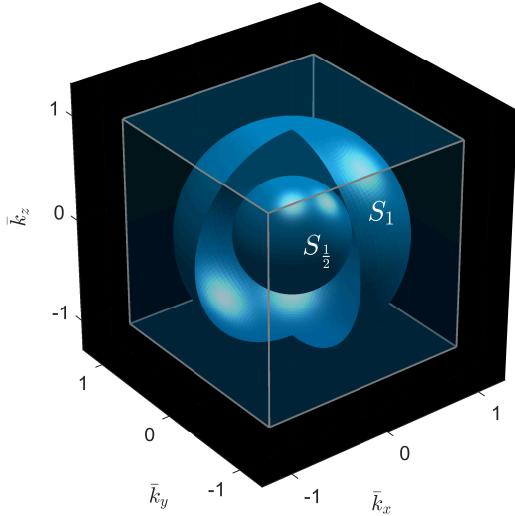


Fig. 1. Unit wave vector cell and spherical regions S_1 and $S_{1/2}$.

Depending on the choice of stencil, temporal and spatial accuracy can be as high as desired [22], [23]. The basic seven-point scheme results from the choice $\mathbf{v}_1 = [1, 0, 0]$, $b_1 = 1$.

The interpolant $\mathcal{I}(\mathbf{x}_{\text{out}})$ is a linear operator returning a scalar pressure signal p_{out}^n from the grid function p_1^n ; various choices will be described in detail in Sections III and IV.

A. Wave Domain

The behaviour of scheme (2) can be analyzed using Fourier techniques, or elementary plane wave solutions of the form

$$p_1^n = e^{i(\omega n T + \mathbf{k} \cdot \mathbf{X})} = e^{i\pi(\bar{\omega} n + \bar{\mathbf{k}} \cdot \mathbf{1})} \quad (4)$$

Here $\omega \in [-\pi/T, \pi/T]$ is an angular frequency and \mathbf{k} is the wave vector. An equivalent form in terms of normalized frequency $\bar{\omega} = T\omega/\pi$ and wave vector $\bar{\mathbf{k}} = X\mathbf{k}/\pi$ is given above; such forms will be used in the remainder of this article. In the source-free case, the insertion of such a solution into (2) leads to a dispersion relation of the form

$$\bar{\omega} = \bar{\omega}(\bar{\mathbf{k}}) \quad \text{with} \quad \lim_{\bar{\mathbf{k}} \rightarrow \mathbf{0}} \bar{\omega} = \lambda|\bar{\mathbf{k}}| \quad (5)$$

The limiting expression above corresponds to the exact dispersion relation for the acoustic wave equation. Away from this limit, though, deviations will occur, and wave propagation is dispersive. For a full discussion of numerical dispersion for schemes of the form (2), see [23]. Here it is assumed that (2) produces reliable results over a confidence range defined by $|\bar{\mathbf{k}}| \leq \gamma$, for some γ with $0 < \gamma \leq 1$. Such a range depends on the scheme, and may be defined in a variety of ways (such as, e.g., a maximum deviation in numerical wave speed [24]).

By basic sampling theory, a scheme defined over a regular Cartesian grid can represent, without aliasing, wave vectors in the unit cell $\|\bar{\mathbf{k}}\|_\infty \leq 1$; see Figure 1. For isotropic wave propagation (due, e.g., to a point source), reliable results can only be obtained over the range $|\bar{\mathbf{k}}| \leq 1$, defining the largest spherical region inscribed within the unit cell, labelled as S_1

in Figure 1. From the above, and for optimisation purposes, the general spherical wave vector range S_γ is defined by

$$S_\gamma = \{\bar{\mathbf{k}} \in \mathbb{R}^3 \mid |\bar{\mathbf{k}}| \leq \gamma\} \quad \text{for} \quad 0 < \gamma \leq 1 \quad (6)$$

III. INTERPOLANTS OVER A SINGLE TIME LEVEL

As a first step, write the interpolation location \mathbf{x}_{out} as

$$\mathbf{x}_{\text{out}} = (\mathbf{l}_{\text{out}} + \boldsymbol{\alpha}) X \quad (7)$$

Here, \mathbf{l}_{out} is an integer 3-vector, and $\boldsymbol{\alpha} = [\alpha_x, \alpha_y, \alpha_z]$ is a 3-vector representing the fractional part of \mathbf{x}_{out} relative to the grid, satisfying $0 \leq \alpha_x, \alpha_y, \alpha_z < 1$. An interpolant $\mathcal{I}(\mathbf{x}_{\text{out}}) = \mathcal{I}^{(0)}(\mathbf{x}_{\text{out}})$, defined over a general set of grid points $\mathbb{I} \subset \mathbb{Z}^3$, and at a single time level behaves as an inner product:

$$\mathcal{I}^{(0)}(\mathbf{x}_{\text{out}}) p_1^n = \sum_{\boldsymbol{\xi} \in \mathbb{I}} a_{\boldsymbol{\xi}}(\boldsymbol{\alpha}) p_{\mathbf{l}_{\text{out}} + \boldsymbol{\xi}}^n \quad (8)$$

Some interpolants satisfy a partition of unity (PoU) property:

$$\sum_{\boldsymbol{\xi} \in \mathbb{I}} a_{\boldsymbol{\xi}}(\boldsymbol{\alpha}) = 1 \quad (9)$$

When the interpolant is reframed as an approximation to a Dirac delta function (after a scaling by $1/X^3$), PoU corresponds to the first discrete moment condition [25]. If PoU is not satisfied, then the interpolant will produce incorrect results in the limit of low frequencies or wavenumbers.

If N_0 is the number of grid locations in \mathbb{I} , it is useful to order the locations as $\boldsymbol{\xi}_1, \dots, \boldsymbol{\xi}_{N_0}$, and then write the corresponding coefficients as a vector $\mathbf{a} = [a_{\boldsymbol{\xi}_1}, \dots, a_{\boldsymbol{\xi}_{N_0}}]^T$.

A. Wave Domain

Under Fourier transformation, and centering about $\mathbf{x} = \mathbf{x}_{\text{out}}$, the interpolator behaves as a multiplier $\hat{\mathcal{I}}^{(0)}$:

$$\hat{\mathcal{I}}^{(0)}(\bar{\mathbf{k}}, \boldsymbol{\alpha}) = \sum_{\boldsymbol{\xi} \in \mathbb{I}} a_{\boldsymbol{\xi}} e^{i\pi \bar{\mathbf{k}} \cdot (\boldsymbol{\xi} - \boldsymbol{\alpha})} \quad (10)$$

A useful measure for error visualisation is the maximum deviation from the ideal of 1 over all propagation directions, for a given wavenumber $\bar{k} = |\bar{\mathbf{k}}|$ and fractional index $\boldsymbol{\alpha}$:

$$E_{\text{max}}(\bar{k}, \boldsymbol{\alpha}) = \max_{|\bar{\mathbf{k}}| = \bar{k}} |1 - \hat{\mathcal{I}}^{(0)}(\bar{\mathbf{k}}, \boldsymbol{\alpha})| \quad (11)$$

It is also normally the case that this error measure is maximal at the fractional index $\boldsymbol{\alpha} = [0.5, 0.5, 0.5]$.

B. Regions

A usual local interpolation region $\mathbb{I}_{\square}^{(M)}$ is box-shaped, consisting of $(2M)^3$ points, for integer $M \geq 1$. It may be defined, in terms of the set $\mathbb{U}^{(M)} = \{-M+1, \dots, M\}$ as

$$\mathbb{I}_{\square}^{(M)} = \mathbb{U}^{(M)} \times \mathbb{U}^{(M)} \times \mathbb{U}^{(M)} \quad (12)$$

A more natural choice, in the case of isotropic wave propagation problems, is the spherical region of radius R grid points:

$$\mathbb{I}_{\circ}^{(R)}(\boldsymbol{\alpha}) = \{\mathbf{z} \in \mathbb{Z}^3 \mid |\mathbf{z} - \boldsymbol{\alpha}| \leq R\} \quad (13)$$

Here, $R > 0$ is any real value, and the resulting point cloud depends on the interpolation fractional index $\boldsymbol{\alpha}$. See Figure 2.

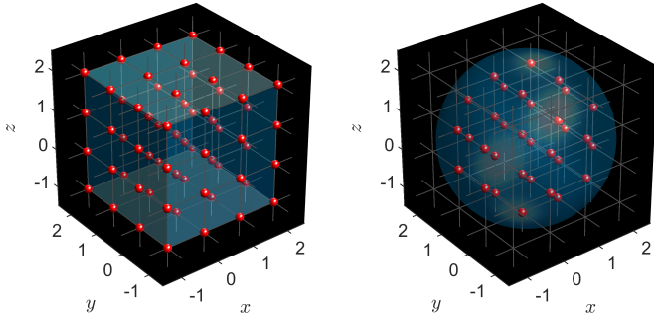


Fig. 2. Regions $\mathbb{I}_{\square}^{(2)}$ (left), and $\mathbb{I}_{\circ}^{(2)}$ (right).

C. Polynomial and Windowed Sinc Interpolants

There are many varieties of polynomial interpolants used in practice. One family, defined over the region $\mathbb{I}_{\square}^{(M)}$, can be written in terms of a polynomial

$$\sum_{\sigma_x=0}^{2M} \sum_{\sigma_y=0}^{2M} \sum_{\sigma_z=0}^{2M} w_{\sigma_x, \sigma_y, \sigma_z} \beta_x^{\sigma_x} \beta_y^{\sigma_y} \beta_z^{\sigma_z} \quad (14)$$

to be evaluated at $[\beta_x, \beta_y, \beta_z] = \alpha$ in order to yield an interpolated value. The $(2M)^3$ coefficients $w_{\sigma_x, \sigma_y, \sigma_z}$ can be written as linear combinations of the grid function values $p_{\mathbf{i}_{\text{out}} + \xi}^n$, $\xi \in \mathbb{I}_{\square}^{(M)}$ [26] (though there are many other possibilities, usually involving matching derivatives of the field data, if available [20]). The cases $M = 1$ and $M = 2$ correspond to trilinear and tricubic interpolants, respectively.

Another popular approach to interpolation in 3D is to employ a separable product of 1D kernels of the form

$$a_{\xi}(\alpha) = a_{\xi_x}(\alpha_x) a_{\xi_y}(\alpha_y) a_{\xi_z}(\alpha_z) \quad (15)$$

for $\xi \in \mathbb{I}_{\square}^{(M)}$. One possibility is the ideal interpolant (the sinc function) with a finite length window applied to it. Lanczos interpolation is one choice [27]:

$$a_{\xi_w}(\alpha_w) = \text{sinc}(\xi_w - \alpha_w) \text{sinc}((\xi_w - \alpha_w)/M) \quad (16)$$

for $w = x, y, z$. Many other choices of window function are possible, as well as the use of piecewise polynomials (splines) approximating the ideal interpolant [28].

See Figure 3 for illustrations of the interpolation error $E_{\max}(\bar{k})$ (11) for these families of interpolants. For Lanczos interpolants, E_{\max} does not approach 0 in the limit as $\bar{k} \rightarrow 0$, reflecting the violation of PoU (9).

D. Optimised Interpolants

In the context of virtual acoustics, it is useful to frame the interpolant design problem in terms of a least squares problem over the confidence range for the particular numerical method employed. To this end, consider the cost function defined by

$$C(\mathbf{a}, \alpha, \gamma) = \iiint_{S_{\gamma}} |1 - \hat{\mathcal{I}}|^2 d\bar{\mathbf{k}} \quad (17)$$

A linear system

$$\mathbf{A}\mathbf{a}^* = \mathbf{b} \quad (18)$$

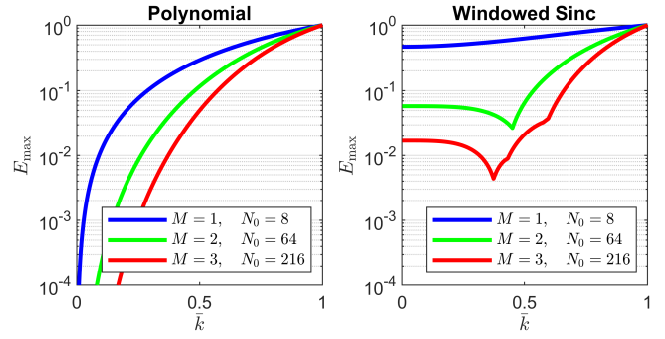


Fig. 3. Maximum interpolation error $E_{\max}(\bar{k})$ for polynomial interpolants (left) and windowed sinc interpolants (right), for order M as indicated. Error is evaluated in the worst case of $\alpha = [0.5, 0.5, 0.5]$.

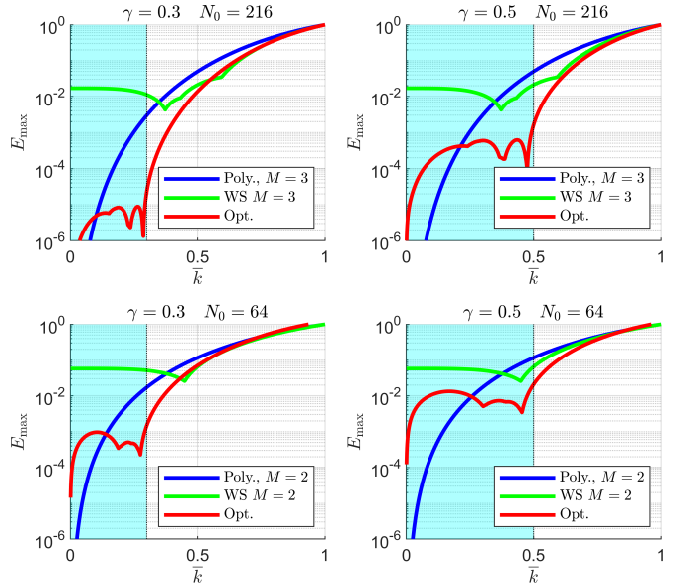


Fig. 4. Maximum interpolation error $E_{\max}(\bar{k})$ for polynomial interpolants, windowed sinc interpolants (WS) and an optimized interpolant, for $N_0 = 216$ points (top row) and $N_0 = 64$ (bottom row). Optimized designs are obtained for $\gamma = 0.3$ (left column) and $\gamma = 0.5$ (right column). Error is evaluated in the near-worst case of $\alpha = [0.52, 0.48, 0.51]$.

results, where $\mathbf{a}^*(\alpha, \gamma)$ are the coefficients that minimize the cost function in (17). Due to the symmetry of the integration domain S_{γ} , the entries of $\mathbf{A}(\gamma)$ and $\mathbf{b}(\alpha, \gamma)$ are available as:

$$[\mathbf{A}]_{rs} = \frac{j_1(\pi\gamma|\xi_r - \xi_s|)}{|\xi_r - \xi_s|} \quad [\mathbf{b}]_r = \frac{j_1(\pi\gamma|\xi_r - \alpha|)}{|\xi_r - \alpha|} \quad (19)$$

where j_1 is a first order spherical Bessel function of the first kind. Property (9) is employed as an additional constraint.

Error plots are shown in Figure 4, for different wavenumber ranges γ , and compared against polynomial and windowed sinc designs for a fixed value of N_0 (216 and 64), corresponding to extremely compact interpolators. Here, a slightly off-center interpolation position is chosen in order to allow greater freedom in the choice of N_0 , allowing a fair comparison with polynomial/sinc interpolants, for which N_0 is fixed. The main effect is that the error is now more evenly distributed over the selected wavenumber range, with polynomial interpolants performing better in the extreme low wavenumber range.

IV. INTERPOLANTS OVER MULTIPLE TIME LEVELS

In an acoustic simulation setting, grid functions are time series, and thus additional information is available for interpolation. A general time-symmetric interpolant $\mathcal{I}^{(Q)}$, operating on $2Q + 1$ time levels for integer $Q \geq 0$, can be defined as

$$\mathcal{I}^{(Q)}(\mathbf{x}_{\text{out}})p_1^n = \sum_{q=0}^Q \sum_{\xi \in \mathbb{I}} \frac{1}{2} a_{\xi,q} \left(p_{\xi}^{n+q} + p_{\xi}^{n-q} \right) \quad (20)$$

Again, under Fourier transformation, or when applied to a solution of the form (4), the interpolant behaves as a multiplier:

$$\hat{\mathcal{I}}^{(Q)}(\bar{\mathbf{k}}, \bar{\omega}, \alpha) = \sum_{q=0}^Q \sum_{\xi \in \mathbb{I}} a_{\xi,q} e^{i\pi \bar{\mathbf{k}} \cdot (\xi - \alpha)} \cos(\pi \bar{\omega} q) \quad (21)$$

But, if we assume that dispersion error is within the confidence range of the FDTD scheme being used, we can employ the limiting form of the dispersion relation given in (5) to arrive at an expression dependent only on the spatial wave vector:

$$\hat{\mathcal{I}}^{(Q)}(\bar{\mathbf{k}}, \alpha) \approx \sum_{q=0}^Q \sum_{\xi \in \mathbb{I}} a_{\xi,q} e^{i\pi \bar{\mathbf{k}} \cdot (\xi - \alpha)} \cos(\pi \lambda |\bar{\mathbf{k}}| q) \quad (22)$$

The interpolant now includes $N_Q = (Q + 1)N_0$ coefficients $a_{\xi,q}$ that can be consolidated as a vector $\mathbf{a} = [a_{\xi_1,q_1}, \dots, a_{\xi_{N_Q},q_{N_Q}}]^T$. Again using the cost function (17), now with the multilevel interpolant given in (22), a linear system of the form (18) again results. The entries of \mathbf{A} and \mathbf{b} are again available in a generalized closed form as:

$$[\mathbf{A}]_{rs} = \sum_{m=0}^3 \frac{j_1(\pi \gamma (\xi_{\Delta,rs} + \sqrt{2}\lambda (C_m q_r + S_m q_s)))}{4\xi_{\Delta,rs}} \quad (23a)$$

$$[\mathbf{b}]_r = \sum_{m=0}^1 \frac{j_1(\pi \gamma (|\xi_r - \alpha| + \sqrt{2}\lambda C_m q_r))}{2|\xi_r - \alpha|} \quad (23b)$$

where $\xi_{\Delta,rs} = |\xi_r - \xi_s|$, $C_m = \cos(\pi(2m+1)/4)$ and $S_m = \sin(\pi(2m+1)/4)$.

For comparison, consider interpolants of varying order Q , but with equal computational cost in terms of additions/multiplications, so that $N = N_0(2Q + 1)$ is held fixed. In Figure 5, E_{max} is plotted, for $N = 216$, and $Q = 0, 1, 2$. Error can be reduced by close to an order of magnitude; as an additional benefit, the spatial range of the interpolant can be made extremely small (for $Q = 2$, the interpolant is confined to a sphere of radius $R = 2.1$ grid points).

V. NUMERICAL RESULTS

As a basic example, consider initialisation with a 3D Gaussian distribution of RMS width 5 cm. Scheme (2) is used, with an 8th order accurate scheme of the ‘‘diamond’’ variety [22], [23] of very low dispersion error, with under 1% error over all propagation directions up to $\bar{k} = 0.62$. The scheme is run at a sample rate of 44100 Hz with $c = 344 \text{ m} \cdot \text{s}^{-1}$ and $\lambda = 1/\sqrt{3}$ over a box of side length 1.2 m. Output is drawn at approximately $\mathbf{x}_{\text{out}} = 1/(4\sqrt{3})[1, 1, 1]$, with $\alpha = [0.52, 0.48, 0.51]$. See Figure 6, illustrating error relative to the exact solution p_{exact} as a function of time t , under different choices of interpolant of size $N = 216$. Relative error is computed as $|1 - p_{\text{out}}/p_{\text{exact}}|$. The behaviour of the interpolants is independent of the choice of initial condition.

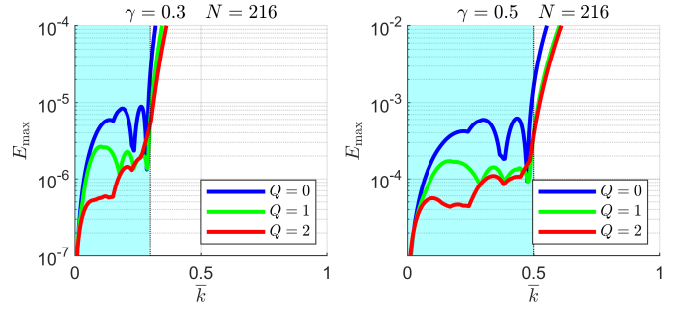


Fig. 5. Maximum interpolation error E_{max} , as a function of wavenumber \bar{k} , for optimized multi-level interpolants with $L = 0, 1, 2$, for $N = 216$ points. Optimized designs are obtained for $\gamma = 0.3$ (left column) and $\gamma = 0.5$ (right column). Error is evaluated in the near-worst case of $\alpha = [0.52, 0.48, 0.51]$.

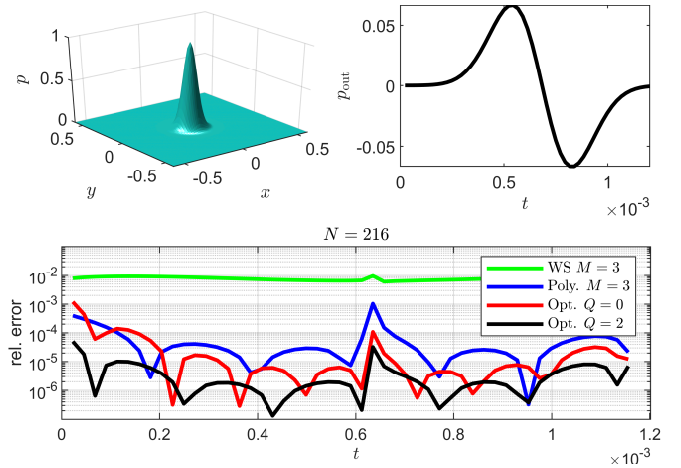


Fig. 6. 2D cross-section of the Gaussian initial condition (top left) and output from coordinates $\mathbf{x}_{\text{out}} = 1/(4\sqrt{3})[1, 1, 1]$ (top right). Bottom: error relative to the exact solution against time for different interpolation techniques, as indicated, with $\alpha = [0.52, 0.48, 0.51]$. All interpolants use $N = 216$ values.

VI. CONCLUDING REMARKS

In this article, a new approach to 3D interpolant design has been demonstrated; performance can be optimised with respect to a specified wavenumber range, and such interpolants are thus well-matched to wave-based acoustic simulation. It has been shown that such optimised interpolants can outperform standard designs over this range in terms of error, sometimes by orders of magnitude, particularly if the inter-dependent nature of solutions to the acoustic wave equation is exploited. Numerical dispersion has been assumed confined outside a scheme-dependent confidence range of wavenumber, and is not employed in the optimisation (though it possible to do so through insertion of the numerical dispersion relation (5) into (22)). When multilevel interpolants are employed, the spatial ‘‘footprint’’ of the interpolant can be made extremely small—a desirable attribute in wave-based acoustics.

The optimisation requires an initial solution of a linear system (similar to the case of polynomial interpolants), and there is thus an additional fixed cost relative to, e.g., windowed sinc interpolants. However, once the interpolant is designed, there is no additional computational cost in the run-time loop.

REFERENCES

- [1] O. Chiba, T. Kashiwa, H. Shimoda, S. Kagami, and I. Fukai, "Analysis of sound fields in three dimensional space by the time-dependent finite-difference method based on the leap frog algorithm," *Journal of the Acoustical Society of Japan*, vol. 49, pp. 551–562, 1993.
- [2] L. Savioja, T. Rinne, and T. Takala, "Simulation of room acoustics with a 3-D finite-difference mesh," in *Proceedings of the International Computer Music Conference*, Århus, Denmark, sep 1994, pp. 463–466.
- [3] D. Botteldooren, "Acoustical finite-difference time-domain simulation in a quasi-cartesian grid," *Journal of the Acoustical Society of America*, vol. 95, no. 5, pp. 2313–2319, 1994.
- [4] —, "Finite-difference time-domain simulation of low-frequency room acoustic problems," *Journal of the Acoustical Society of America*, vol. 98, no. 6, pp. 3302–3308, 1995.
- [5] S. Bilbao, B. Hamilton, J. Botts, and L. Savioja, "Finite volume time domain room acoustics simulation under general impedance boundary conditions," *IEEE/ACM Transactions on Audio Speech and Language Processing*, vol. 24, no. 1, pp. 161–173, 2016.
- [6] M. Hornikx, W. De Roeck, and W. Desmet, "A multi-domain Fourier pseudospectral time-domain method for the linearized Euler equations," *Journal of Computational Physics*, vol. 231, no. 14, pp. 4759–4774, 2012.
- [7] F. Pind, A. Engsig-Karup, C. Jeong, J. Hesthaven, M. Mejlum, and J. Stromann-Andersen, "Time domain room acoustic simulations using the spectral element method," *Journal of the Acoustical Society of America*, vol. 145, no. 6, pp. 3299–3310, 2019.
- [8] H. Wang, I. Sihar, R. Munoz, and M. Hornikx, "Room acoustics modelling in the time-domain with the nodal discontinuous Galerkin method," *Journal of the Acoustical Society of America*, vol. 145, no. 4, pp. 2650–2663, 2019.
- [9] D. Murphy, A. Kelloniemi, J. Mullen, and S. Shelley, "Acoustic modelling using the digital waveguide mesh," *IEEE Signal Processing Magazine*, vol. 24, no. 2, pp. 55–66, 2007.
- [10] N. Raghuvanshi, R. Narain, and M. Lin, "Efficient and accurate sound propagation using adaptive rectangular decomposition," *IEEE Transactions on Visualization and Computer Graphics*, vol. 15, no. 5, pp. 789–801, 2009.
- [11] K. Kowalczyk and M. van Walstijn, "Room acoustics simulation using 3-D compact explicit FDTD schemes," *IEEE Transactions on Audio Speech and Language Processing*, vol. 19, no. 1, pp. 34–46, 2011.
- [12] "Computational simulation in architectural and environmental acoustics," T. Sakuma, S. Sakamoto, and T. Otsuru, Eds. Springer, 2014.
- [13] C. Manry and S. Broschat, "FDTD simulations for ultrasound propagation in a 2-D breast model," *Ultrasonic Imaging*, vol. 18, pp. 25–34, 1996.
- [14] I. Hallaj and R. Cleveland, "FDTD simulation of finite-amplitude pressure and temperature fields for biomedical ultrasound," *Journal of the Acoustical Society of America*, vol. 105, no. 5, pp. L7–L12, 1999.
- [15] J. Robertson, B. Cox, J. Jaros, and B. Treeby, "Accurate simulation of transcranial ultrasound propagation for ultrasonic neuromodulation and stimulation," *Journal of the Acoustical Society of America*, vol. 141, no. 3, pp. 1726–1738, 2017.
- [16] C. Peskin, "The immersed boundary method," *Acta Numerica*, vol. 11, pp. 479–517, 2002.
- [17] J. Seo and R. Mittal, "A high-order immersed boundary method for acoustic wave scattering and low-mach number flow-induced sound in complex geometries," *Journal of Computational Physics*, vol. 230, no. 4, pp. 1000–1019, 2011.
- [18] A. Kadosh, D. Cohen-Or, and R. Yagel, "Tricubic interpolation of discrete surfaces for binary volumes," *IEEE Transactions on Visualization and Computer Graphics*, vol. 9, no. 4, pp. 580–586, 2003.
- [19] A. Torrado-Carvajal, D. Albrecht, J. Lee, O. Andronesi, E. Ratai, V. Napadow, and M. Loggia, "Inpainting as a technique for estimation of missing voxels in brain imaging," *Annals of Biomedical Engineering*, vol. 49, no. 1, pp. 345–353, 2021.
- [20] F. Lekien and J. Marsden, "Tricubic interpolation in three dimensions," *International Journal for Numerical Methods in Engineering*, vol. 63, pp. 455–471, 2005.
- [21] S. Bilbao and B. Hamilton, "Directional sources in wave-based acoustic simulation," *IEEE/ACM Transactions on Audio Speech and Language Processing*, vol. 27, no. 2, pp. 415–428, 2019.
- [22] J. Tuomela, "On the construction of arbitrary order schemes for the many dimensional wave equation," *BIT Numerical Mathematics*, vol. 36, no. 1, pp. 158–165, 1996.
- [23] S. Bilbao and B. Hamilton, "Higher-order accurate two-step finite difference schemes for the many dimensional wave equation," *Journal of Computational Physics*, vol. 367, pp. 134–165, 2018.
- [24] J. Saarelma, J. Botts, B. Hamilton, and L. Savioja, "Audibility of dispersion error in room acoustic finite-difference time-domain simulation as a function of simulation distance," *Journal of the Acoustical Society of America*, vol. 139, no. 4, pp. 1822–1832, 2016.
- [25] J. Waldén, "On the approximation of singular source terms in differential equations," *Numerical Methods for Partial Differential Equations*, vol. 15, pp. 503–20, 1999.
- [26] E. LaMar, B. Hamann, and K. Joy, "High-quality rendering of smooth isosurfaces," *Journal of Visualization and Computer Animation*, vol. 10, pp. 79–90, 1999.
- [27] T. Moraes, P. Amorim, J. Da Silva, and H. Pedrini, "Medical image interpolation based on 3d Lanczos filtering," *Computer Methods in Biomechanics and Biomedical Engineering: Imaging & Visualization*, vol. 8, no. 3, 2019.
- [28] T. Lehmann, C. Gönner, and K. Spitzer, "Survey: Interpolation methods in medical image processing," *IEEE Transactions on Medical Imaging*, vol. 18, no. 11, 1999.